Contributed paper

OPTO-ELECTRONICS REVIEW **11**(4), 281–289 (2003)

Improvement in silicon thin film solar cell efficiency

A. KOŁODZIEJ*, P. KREWNIAK[1], and S. NOWAK[2]

[1]University of Mining and Metallurgy, Institute of Electronics,
30 Mickiewicza Ave., Kraków, Poland
[2]Institute of Electron Technology, 39 Zabłocie Str., Kraków, Poland

This paper presents the improved method of obtaining the stable hydrogenated amorphous silicon (a-Si:H) due to the protocrystalline nature of the Si:H materials. The latest experiments and results on silicon thin film solar cells are presented in this publication. The relation of microstructure and the efficiency of amorphous and microcrystalline silicon single photovoltaic structures as well as tandem on glass and triple on steel foil solar cell are also discussed.

Keywords: silicon thin film solar cells, hydrogenated amorphous silicon (a-Si:H), microcrystalline silicon, single-, tandem- and triple-junction solar cells, RF PECVD.

1. Introduction

Efficiencies for single junction amorphous a-Si:H and microcrystalline μc-Si cells made by plasma-enhanced chemical vapour deposition (PECVD) have now exceeded 8-10% [1] and multijunction devices with one intrinsic layer μc-Si:H and one intrinsic layer a-Si:H allow for absorption of a greater percentage of the solar spectrum, then with each layer used individually, and give higher efficiency.

It has been reported that hydrogenated microcrystalline silicon (μc-Si:H) solar cells do not show light-induced degradation under prolonged light soaking [2,3]. In addition, the high long wavelength absorption makes μc-Si:H solar cell suitable as a substitute for hydrogenated amorphous silicon-germanium alloy (a-SiGe:H with the higher content of Ge) bottom cell in multijunction structures. Since the first μc-Si:H solar cell reported in 1994 [2], significant progress has been made by using various techniques such as very-high-frequency (VHF) glow discharge [2–4], reactive magnetron sputtering (RMS) [5,6], high power and pressure radio-frequency (RF) glow discharge [7,8], hot-wire CVD [9], and Gas-Jet [10]. Recently, the a-Si:H/μc-Si:H double-junction solar cell with an initial efficiency of 14.1% and an a-Si:H/μc-Si:H hybrid module with an initial efficiency of 11.7% have been reported [11].

The aim of this paper was to find new methods which provide higher efficiency of silicon thin film solar cells in relation to the mentioned above. Depositions were performed on ZnO covered glass substrates and Al/ZnO put on a steel foil. The structures of p-i-n-p-i-n and n-i-p-n-i-p-n-i-p Si:H were studied by cross sectional TEM and XRD analysing. The analyses of FF, V_{oc} and I_{sc} of the structures were also carried out.

The samples were manufactured in Kraków, Poland, and in PennState, USA. The layers were made by means of the reactive magnetron sputtering (RMS) and RF plasma enhancement chemical vapour deposition (RF PECVD). The photovoltaic laboratory was built that contains modern 3-chamber RF PECVD apparatus and also a special system of the gas cabinets with suitable installations. This laboratory is created in a totally new room of 90 m^2 with a modern filtering system that ensures much higher degree of cleanness.

In the series of publications, the authors presented the stages of their work that at the end leaded to the manufacturing of the multilayer solar cells. Research has been performed on:

- the electrode system, among them many on ZnO and ITO layers as well as connection electrodes [6],
- double-side antireflection layers on glass [13],
- the nature of the phase changes: an amorphous silicon – microcrystalline silicon [14,15],
- the thin-layer amorphous silicon pin cell made on glass by means of the sputtering, and also RF PECVD, an efficiency 7% [16],
- the thin-layer pin cell on the microcrystalline silicon, made on glass by means of the sputtering technique and RF PECVD, an efficiency 4.5% [16],
- the photoconductivity, the Staebler-Wronski effect and the degradation of cells [17],
- the silicon solar cell – tandem type – on glass, an efficiency 7.5% [18],
- the layers and silicon pin structures on the stainless steel. The series of triple-junction cells was manufactured on the stainless steel, with efficiency up to 10% [17,19].

*e-mail: kolodzie@agh.edu.pl

2. Film manufacturing

Amorphous samples were fabricated by a conventional capacitatively coupled RF (13.56MHz) PECVD in a multichamber system. The source gas was silane diluted by hydrogen, and diborane or phosphine was used as doping gas. Typical pressure was 0.5 Torr. Other conditions were as follows: RF power was 0.2–0.6 W/cm^2 and anode – cathode distance was 1–2 cm. The rate of layer deposition did not exceed 0.5–0.6 Å/s. Microcrystalline (c-Si:H) samples were deposited under high gaseous pressure conditions in which high quality materials were obtained at a high growth rate up to 5 Å/s. The pressure used in this work was around 2 Torr, it is significantly higher pressure than in conventional conditions. The μc-Si:H *i*-layer were deposited using the following conditions: RF power was varied in the range of 1.0–1.5 W/cm^2, an anode-cathode distance of 1–4 cm, a flow rate of silane in the range of 2–80 sccm, hydrogen dilution of 90–99.5% and the T_s held either at 150°C to 300°C. The back ground pressure of the deposition chamber was less than 2×10^{-7} Torr, whereas the reactor buildup rate is as high as 9×10^{-6} Torr×l/s. In the presented setup, concentration of oxygen was typically 2×10^{19} cm^{-3} in non-doped c-Si:H films, and this value was independent of the deposition temperature of 200–250°C [12]. The a/μc Si:H samples were prepared in the area (10×10 cm) system situated on the anode side of the RF electrode.

The new specially configured RF PECVD three-chamber apparatus was built at the Electronic Department in Kraków. It makes possible to obtain not only amorphous and microcrystalline silicon films but also polycrystalline Si films. The substrate temperature can be changed from 20°C to 700°C. Parts of the apparatus are presented in Fig. 1.

The solar cell surface areas were from 0.25 cm^2 to 18.0 cm^2. The growth conditions of a/μc i-layer were varied to optimise the device performance. The choice of optimal amorphous and microcrystalline layer deposition temperature and other parameters results from analysis of the characteristics shown in Figs, 2, 3, 4, 5, 7, and 8.

3. Microstructural phase transitions in Si:H films

Fabrication of the intrinsic layers using PECVD with moderate hydrogen dilution of silane allowed for a significant progress in improving the performance and stability of a-Si:H based p-i-n and n-i-p solar cells.

The thin film of a-Si:H prepared under H_2-dilution conditions, $R = [H_2]/[SiH_4]$ – depending on substrate and RF power – evolves from the amorphous phase to a mixed (a + μc)-Si:H phase and to a single phase with a thickness shown in Fig. 2. Likewise, a significant progress was

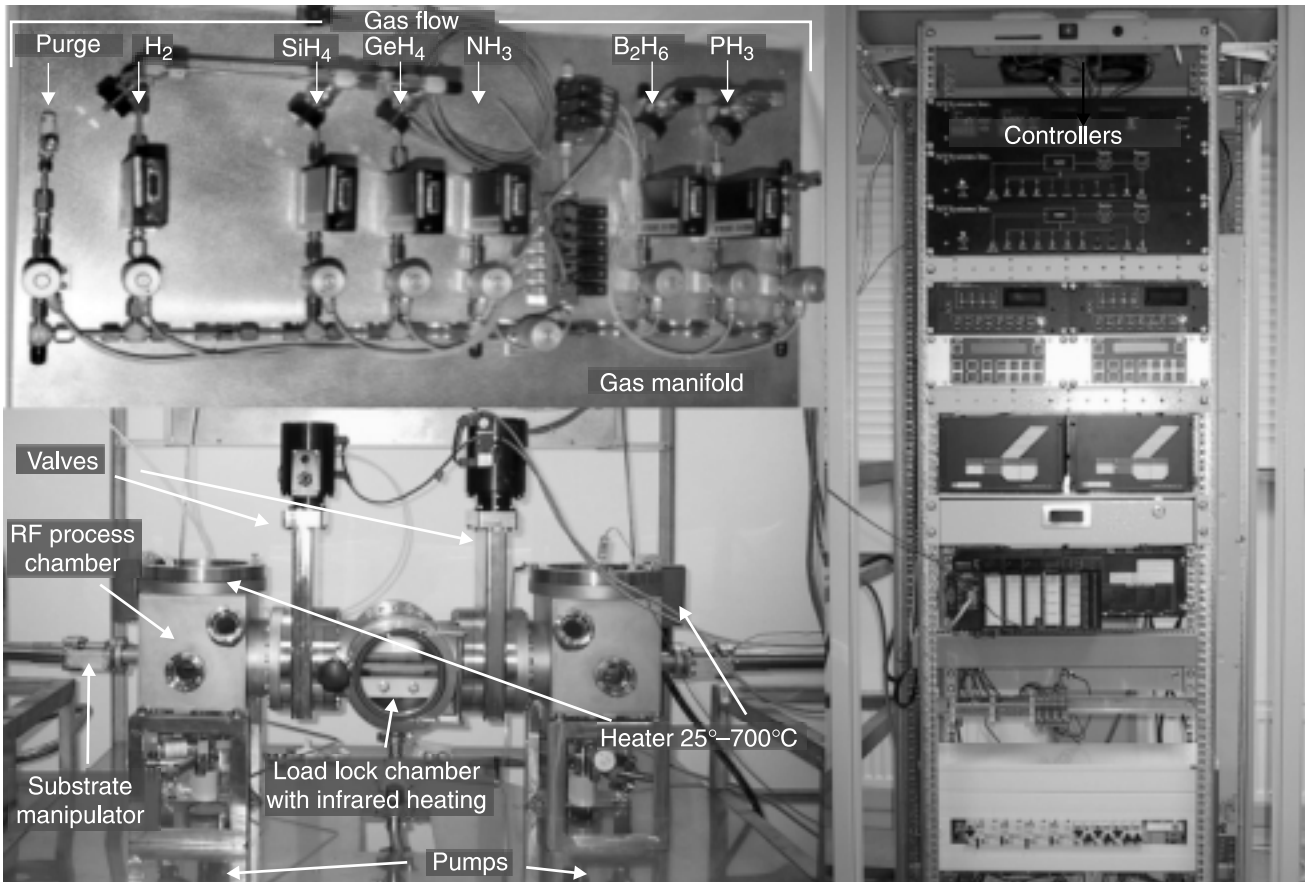

Fig. 1. Parts of the RF PECVD apparatus made by authors (not in a scale).

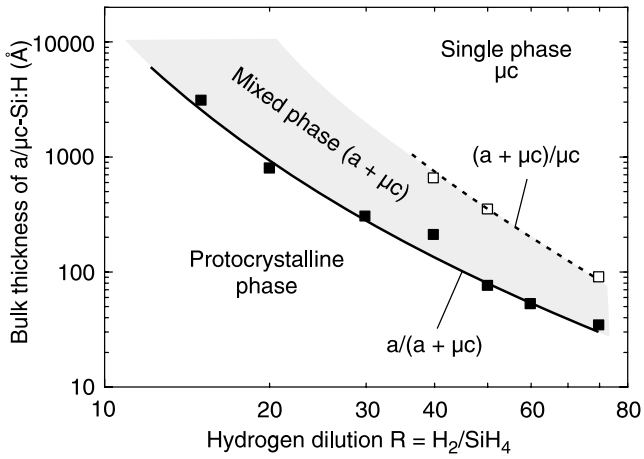

Fig. 2. The film thickness d_b, at which the different phase transitions occur during Si:H film growth in RF PECVD normal process, plotted as a function of the hydrogen dilution ratio $R = H_2/SiH_4$ using glass substrate.

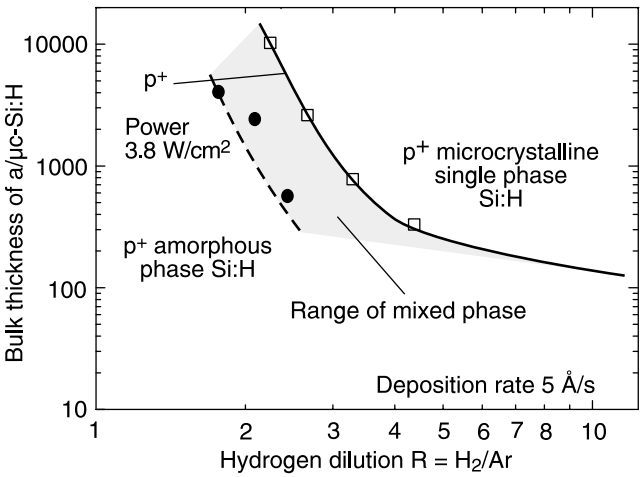

Fig. 3. The film thickness d for the phase transition from a-Si:H to μc-Si:H, for p^+ and "i" RMS films, plotted against the hydrogen dilution ratio of Ar. The range of mixed a-μc or coalescent clusters was separated from the microcrystalline range.

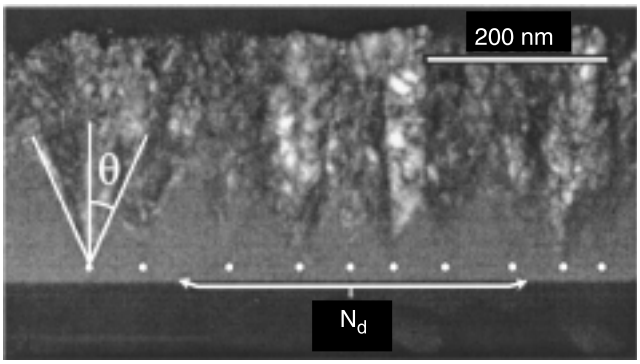

Fig. 4. Cross-sectional transmission electron microscopy image for the final $R = 20$ Si:H deposition. Indicated a representative conical microcrystalline structure, and the points near the substrate interface identifying the nuclei from which the nucleation density is estimated.

achieved, particularly in p^+ and n^+ layer manufactured by a RMS method with the changed hydrogen content in a gas mixture (Fig. 3).

Conditions of high hydrogen dilution (single phase) for all sputterings of the doped films can be seen just above R 10 (= H_2/Ar) for typical 200 Å thickness of the p^+ layer (Fig. 3) [15], whereas in the case of PECVD such conditions appear at R 40 (= H_2/SiH_4).

In these diagrams, the Si:H bulk layer thicknesses at which these transitions occur can be plotted as continuous functions of a key deposition variable that is used to control the phase, typically the H_2-to-SiH_4 gas flow ratio R.

The phase diagram depends not only on the other fixed deposition conditions, such as plasma power, substrate temperature, and total gas pressure, but also on the substrate since the latter exerts a strong influence over crystallite nucleation. Deposition phase diagrams are very convenient in the design of devices since they describe the regimes of layer thickness and deposition parameter space within which single-phase a-Si:H, (a + μc)-Si:H and single-phase μc-Si:H are obtained. As a review of such phase diagrams Fig. 5 shows the proposed schematic structure of ~5000 Å thick Si:H films on $R = 0$ a-Si:H substrate films, given as a continuous function of R along with the thicknesses of the a→(a + μc) and (a + c)→μc transition boundaries. In such structures, the cone angle for crystallite growth is relatively constant at 15–20° (Fig. 4) and the nucleation density increases rapidly when increasing R [20].

Correlations of the phase diagrams for intrinsic Si:H layers with the corresponding electronic properties and p-i-n device performance demonstrate that the optimum i-layers are obtained at the maximum possible R value for the desired thickness without crossing the a→(a + μc) boundary of the phase diagram into the mixed-phase growth regime. It should be emphasized that because the R value at this phase boundary depends on both the nature of the substrate and the i-layer thickness. These aspects of the materials or device structure must be specified in order to identify the optimum conditions. For i-layers deposited on amorphous film substrates (such as the p or n-layers of p-i-n or n-i-p solar cells), the optimum a-Si:H

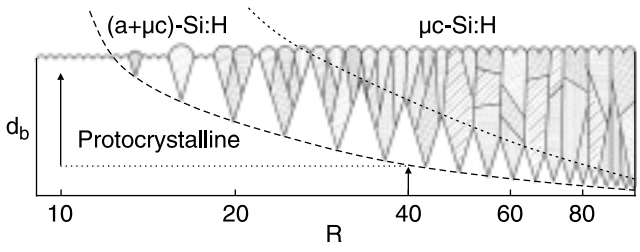

Fig. 5. Schematic of the structure of Si:H films prepared as a function of R. The dashed and dotted lines identify the a→(a + c), and (a + c)→ c transitions, respectively. The arrows denote Si:H i-layer process found to optimise the performance of p-i-n solar cells.

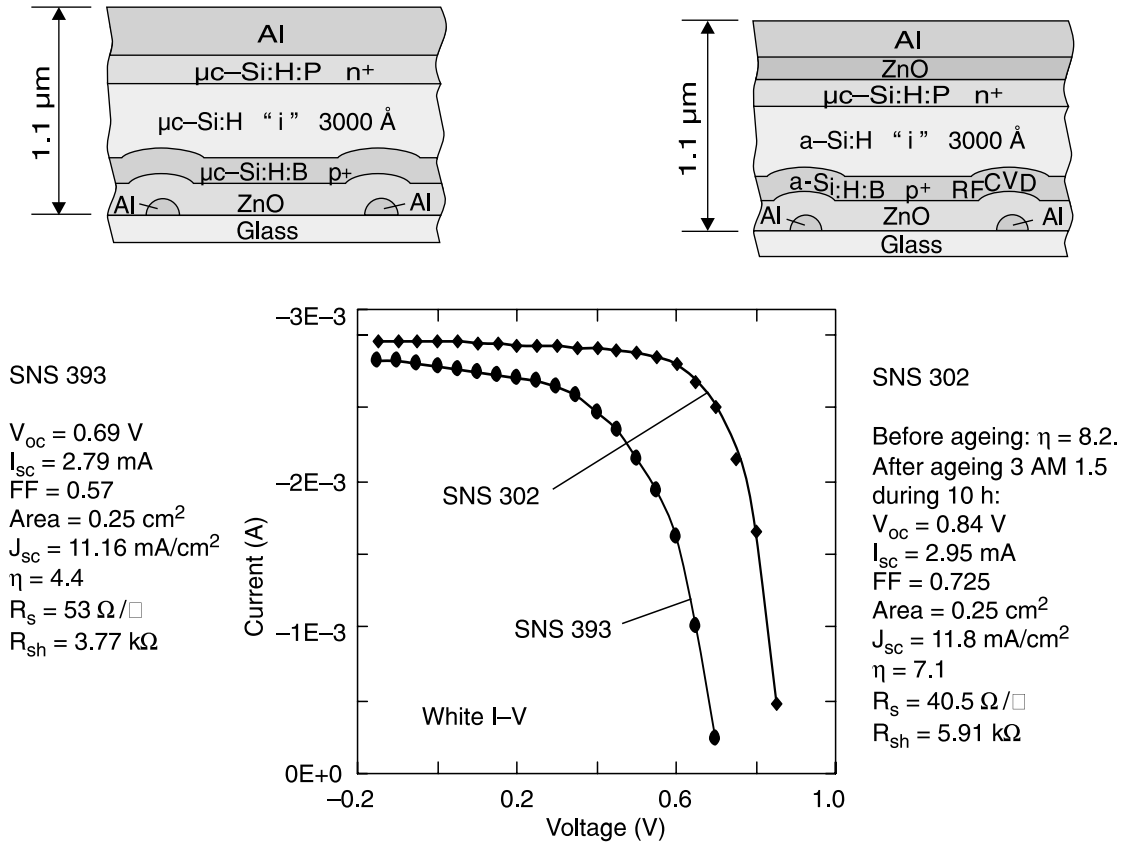

Fig. 6. Schematic multilayer structure and I–V characteristic of solar cell with area of 0.25 cm^2 manufactured on the basis of microcrystalline (SNS 393) or amorphous (SNS 302) silicon layer as well as ZnO:Al and p$^+$ layer obtained by RFCVD method.

i-layer material has been described as protocrystalline Si:H. As its name implies, protocrystalline Si:H ultimately evolves into (a + μc)-Si:H if the film is allowed to grow beyond the desired thickness for which the deposition process was optimised. The unique characteristic of protocrystalline Si:H is its higher stability to light inducing degradation when measured for both materials and devices. Finally, because the a→(a + μc) transition decreases in thickness with increasing R, two-step and even multi-step i-layer processes can be designed on the basis of the phase diagram in order to optimise solar cells. Performance levels beyond those accessible in one-step processes were demonstrated.

4. Amorphous and crystalline single junction solar cells

With respect of these, amorphous Si:H films were deposited in the multichamber system in normal RFCVD conditions with H_2 dilution less than 14:1. Simple solar cell structures of p-i-n and n-i-p configuration were fabricated onto ZnO/ITO coated glass with the p-type material fabricated using a SiH_4, CH_4, and B_2H_6 gas mixture. The typical properties of the wide band gap "p" material were a Tauc optical gap of 1.9 eV and a photoconductivity of ~2×10^{-6} (Ω cm)$^{-1}$. The n$^+$ layer was prepared using a SiH_4 and PH_3 gas mixture. The resultant n$^+$ material exhibited a dark conductivity of 2×10^{-3} (Ω cm)$^{-1}$.

The microcrystalline i-type layers with the thickness of 1 m or 0.3 m were manufactured under the modified RFCVD conditions (a two-step process). A rule was that the initial 10–20 Å were made under increased H_2 dilution up to 200:1, and then returned back to the conditions where H_2 dilution was about 14:1. The choice of these conditions was made on the basis of the analysis of characteristics shown in Figs. 2, 3, 4, and 5.

The analyses were carried out on the basis of the cross section TEM pictures of the structure of stainless steel/Al-ZnO/n$^+$/i-μc Si so as to control the incubation layer of the microcrystalline films (to be published). Using this method of deposition we limited the amorphous layer in relation to the one made without special recipe. This, in turn, limited a negative influence of the amorphous incubation layer.

Microcrystalline p-i-n or n-i-p structures inside solar cell structures were constructed with the μc p-type material fabricated using a SiH_4, H_2, and Trimethylboron gas mixture. The typical dark conductivity of the c p-type material was 8×10^{-2} (Ω cm)$^{-1}$. The μc n$^+$ layer was prepared using a SiH_4, H_2, and PH_3 gas mixture which exhibited a dark conductivity of 1 (Ω cm)$^{-1}$. The devices were deposited onto ITO coated glass with a thin layer of ZnO of 9 Ω V.

The ZnO layer was deposited using DC-sputtering of Al-doped Zn. The texture of the ZnO:Al substrates was formed by the wet etching process and the surface morphology was varied by changing etching time. Surface morphology of the substrates and films are controlled by the atomic force microscopy (AFM) [5].

Subsequent layers which constitute the solar cells, obtained by means of the RMS, create the mixed interlayers that diminish the carrier mobility and conductance of this structure, because of additional defects and recombinations centres. Therefore usage of the ZnO:Al/p$^+$ a-Si:H structure has a great advantage over ITO/p$^+$ a-Si:H structures because the layers of ZnO:Al are more hermetic and resistant to diffusion and chemical mixing with the overlapping layer, i.e., p$^+$ a-Si:H. The Zn:O layers expose features of a semiconductor layer which can create an efficient heterojunction with a p$^+$/i a-Si:H layer and thus influence the distribution on the electrical field in the structure of a cell. We provided the manufacturing condition of the glass/ZnO:Al and p$^+$ a-Si:H on ZnO:Al films by RMS in Refs. 13 and 14.

Not only the base crystallization of i a-Si:H during RF PECVD process is essential, but also the nature of influence of ZnO/p$^+$ on a-Si:H crystallization, as well as its influence on performance of the p-i-n a-Si:H solar cell. A precise control of obtaining the amorphous and microcrystalline p$^+$ silicon layer was worked out [15,16]. We indicated that single crystallized p$^+$ layer forced Si i-layer crystallization to the depth of about 70 nm. This negatively influences the amount of light that reaches the active zone of the cell, and diminishes V_{bi} and V_{OC} as well. Exemplary results of the influence of the bottom p$^+$ layer on crystallization of the i-layer are contained in Ref. 16. For the influence study we used interference Bragg analysis of the multilayer system.

A current-voltage I-V characteristics of the fabricated solar cells were measured under the conditions of AM1.5, 100 mW/cm^2, and 25°C.

5. Metastability

The analysis of the effusion velocity in the vacuum conditions of 10^{-8} Torr and leakage not exceeding 10^{-6} Torr×l/s in dependence on temperature show, at the one hand – the stability regions of the material, and at the other – the temperature thresholds that need to be overcome to result in full policrystallisation of the silicon layer (Figs. 7 and 8). In accordance with those data, the poly-Si structure with the triple junction was manufactured.

On the other hand, a significant reduction in photodegradation of solar cells was achieved by using hydrogen dilution of silane-processing gas during film growth [21]. Beyond a certain dilution threshold value, the silicon films become microcrystalline. Shortly before achieving this threshold one observes evidence of greater structural order or substantial regions of intermediate range order [22] in the amorphous film [23,24]. Transmis-

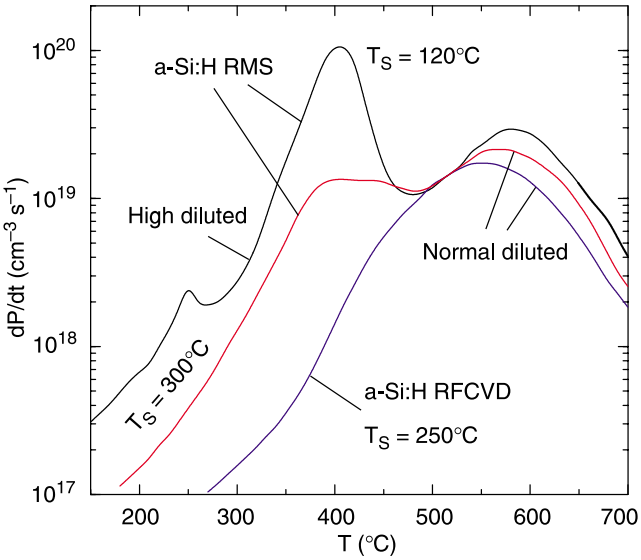

Fig. 7. The hydrogen effusion velocity vs. temperature for silicon layers obtained by the RFCVD and RMS methods for various hydrogen content in a layer. A dependence of the effusion velocity for amorphous layers is also shown.

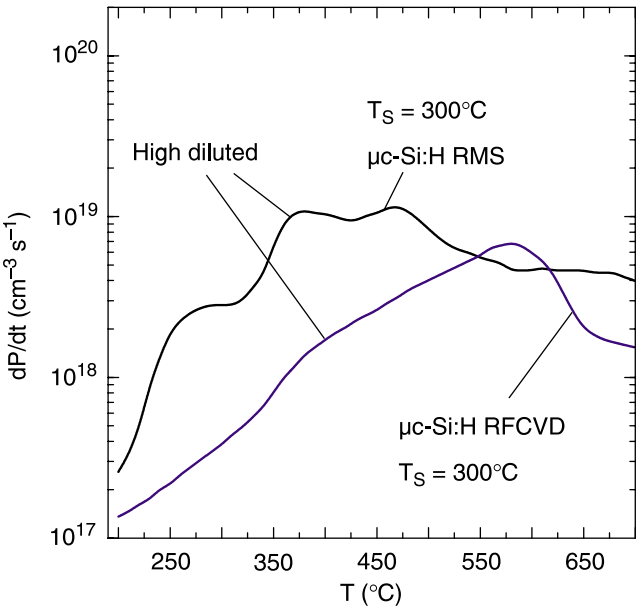

Fig. 8. The hydrogen effusion velocity vs. temperature for silicon layers obtained by the RFCVD and RMS methods for various hydrogen content in layer. A dependence of the effusion velocity for microcrystalline layers is also shown.

sion electron micrographs show regions that have a crystalline-like appearance. This produces no microcrystalline X-far diffraction peaks, but a narrowing of the amorphous Si (111) peak. In addition to the transverse optical (TO) vibration band near 475 cm^{-1}, one finds in the Raman spectra a TO band at 490 cm^{-1} that grows with the fraction of the ordered regions. Despite the dilution ratios R of 20:1 and larger, the total H concentrations in the RF plasma-deposited films remains near 8–10 at. %. How-

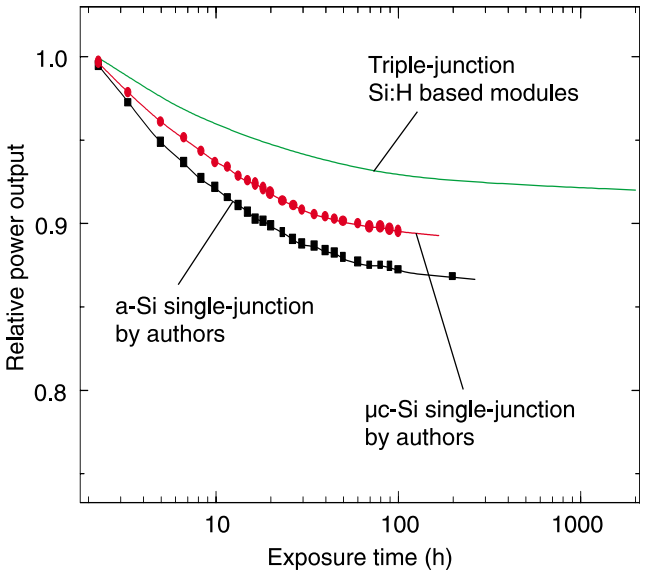

Fig. 9. Normalized solar cell output for a single-junction (after authors) and multijunction (after NREL data) devices illustrating the enhanced stability for multijunction devices.

ever, the distribution of H becomes more heterogeneous with the ordered regions containing less H and the surrounding amorphous material proportionately more. The shift of the Si-H wagging mode from 635–640 cm^{-1} to about 620 cm^{-1} observed in the infrared spectra of near-threshold material [24] suggests a change toward a surface-type Si-H bonding environment. Presumably, this gives rise to the sharp peak near 400°C in the hydrogen effusion spectrum [25] (Figs. 7 and 8).

These amorphous films already crystallize near 550°C – a temperature significantly below the 650°C crystallization temperature of films grown without H dilution. The amorphous-microcrystalline phase boundary depends not only on the dilution ratio R but also on the film thickness d, as shown in Fig. 5, because the ordered regions grow with the growing film [26]. Other parameters affecting the evolutionary phase boundary are: a substrate material, deposition rate and temperature, and the frequency (13.6 or 80 MHz, or microwave) of the plasma-deposition process. A sudden decrease in the open circuit voltage is a useful signal that the i-layer thickness has exceeded the phase boundary when the film is incorporated in a solar cell [27]. As a fraction of amorphous-ordered regions increases with film thickness before the microcrystalline borderline, the dangling bond concentration decreases [28]. This spatial variation suggests that optimised a-Si:H films might be obtained by varying (decreasing) the H dilution during a growth. Eight to ten percentage of H is far more than needed to saturate potential dangling bonds. Because H diffusion decreases with H concentration, one also expects the SWE to diminish.

In Fig. 9, the comparison of the photodegradation of the single-junction and multi-junction cells is presented. It describes the subsequent processes put forth in this work that lead to a decrease in photodegradation.

6. Experiments with tandem on glass and triple junctions solar cells

The exemplary I–V characteristics, as well as a view and the layered structure of tandem cells made by the authors, are shown in Figs. 10, 11, and 12.

It can be observed that the tandem structures manifest good V_{oc} but much worse FF and J_{sc} in comparison to single structures.

In the triple-junction cells, shown in Figs. 13 and 14 – looking from the side of light incidence – despite of an amorphous a-Si:H p-i-n structure, the second amorphous a-Si:H p-i-n structure was used, but with a small dope of GeH4, i.e., less than 1%. The two gave a high total V_{OC} round 1.7 eV.

As a third structure, the p-i-n silicon single crystal was used, made under temperature 450°C with R = 10. All things considered, the setup is quite innovative, and among ten pieces from the series, a sample with an efficiency of 10.25% was found (Fig. 15).

An analysis of the reasons of small values of the fill factor FF is led using the equations describing the $I(V)$

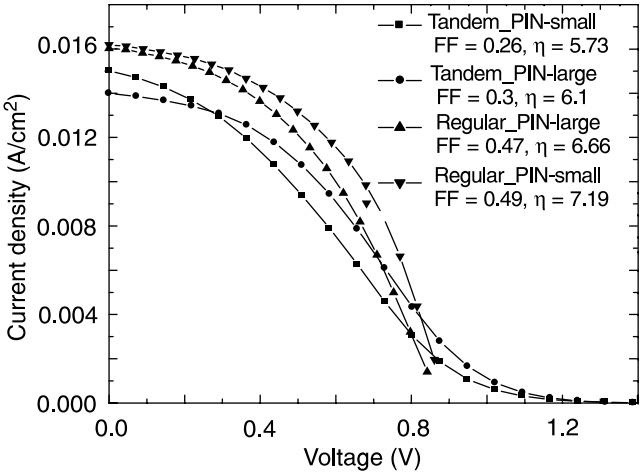

Fig. 10. The comparison of the characteristics of the single junction cell and the double junction cell made on the first one.

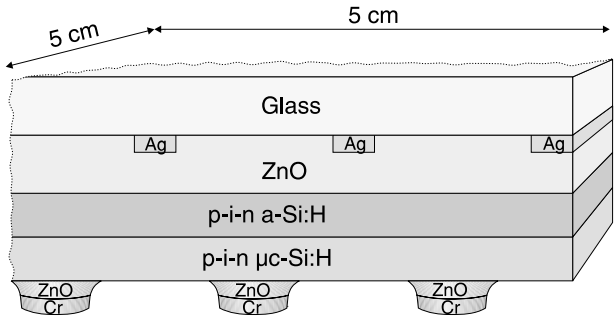

Fig. 11. The layer cross-section of tandem-junction solar cell on glass shown in Fig. 12.

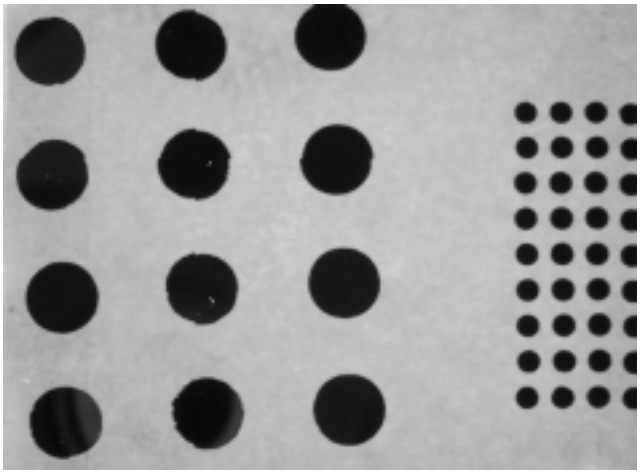

Fig. 12. A view of the experimental structure of a tandem-junction solar cell on glass, made by the authors.

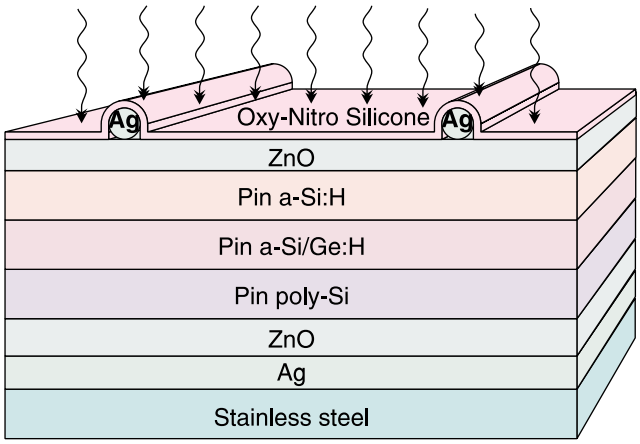

Fig. 13. The layer cross-section of triple-junction cell shown in Fig. 14.

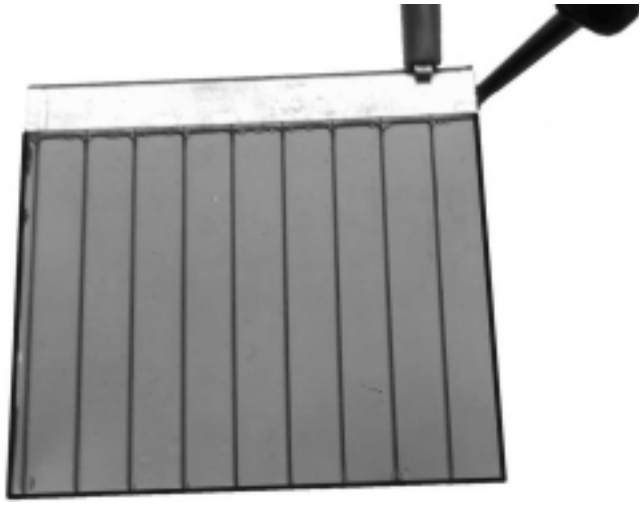

Fig. 14. A view of a triple-junction cell on stainless steel with size of 5×5cm^2, made by authors.

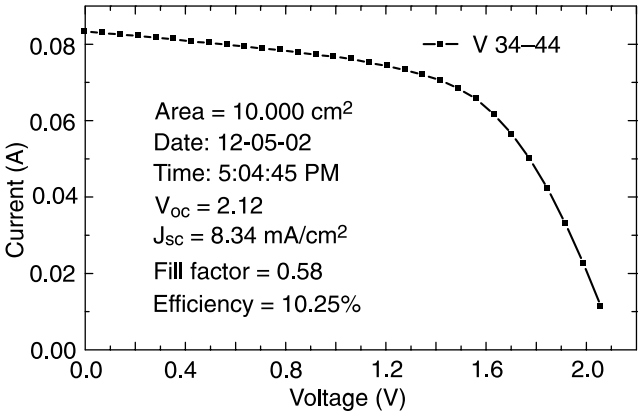

Fig. 15. The I-V characteristic of the best solar cell chosen from the series of triple-junction cells with big area, and its parameters.

characteristics for the following simplified analytical model

$$J(V) = J_{Ph} - J_S\left[\exp\left(\frac{V + JR_S}{nkT}q\right)\right] - J_{rec} - \frac{V + JR_S}{R_{sh}}$$

$$J_{mc} = G_0\left(\frac{1}{\mu_n\tau_n} - \frac{e^{-\,ad_i}}{\mu_p\tau_p}\right)\int_0^{d_i}\frac{1}{E(x)}dx + G_0\left(\frac{1}{\mu_p\tau_p} - \frac{1}{\mu_n\tau_n}\right)\int_0^{d_i}\frac{e^{-\,ax}}{E(x)}dx$$

where J_{Ph} is the photocurrent, J_S is the dark saturation current, J_{rec} is the recombination current in p-i-n a-Si:H diodes, $\mu\tau$ is the product of the hole and electron mobility, $J(V)$ is the current density, R_S is the series resistance, R_{sh} is the shunt resistance, n is the diode ideality factor, k is the Boltzmann's constant, and q is the elementary charge. It is considered in the KBN report No. PBZ KBN 05/T11/98 [17].

The most important question is whether the integral

$$\int\left[\frac{1}{E(x)}\int G(x)dx\right]dx$$

has an analytical solution. Therefore, for the function $E(x)$, the simplest linear function $E(x) = ax + b$ was assumed. It

is a single-exponential model in conjunction with the cited formula for the recombination for a single pin a-Si:H cell. The simulation characteristics for different basic parameters are shown in Figs. 16 and 17.

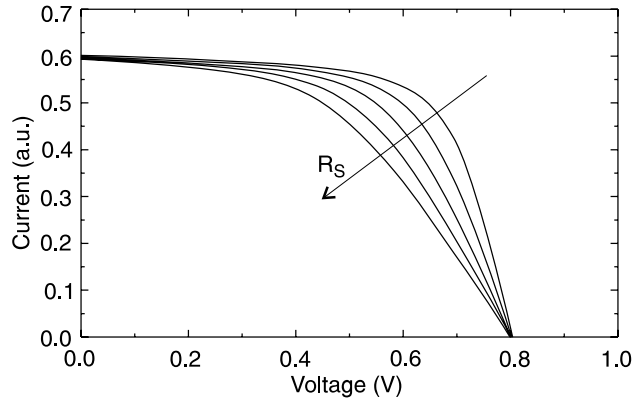

Fig. 16. The group of characteristics for various serial resistance values.

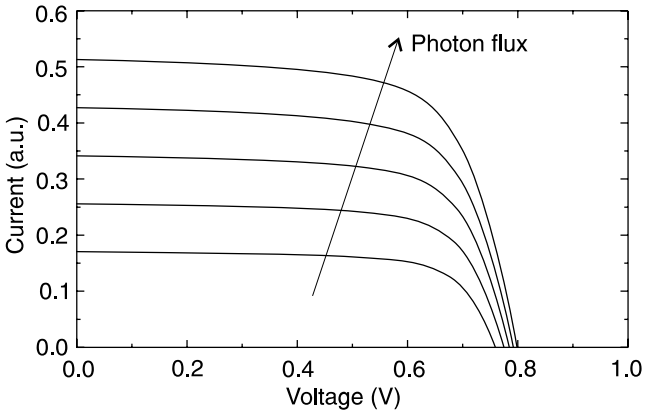

Fig. 17. The group of characteristics for various photon flux values.

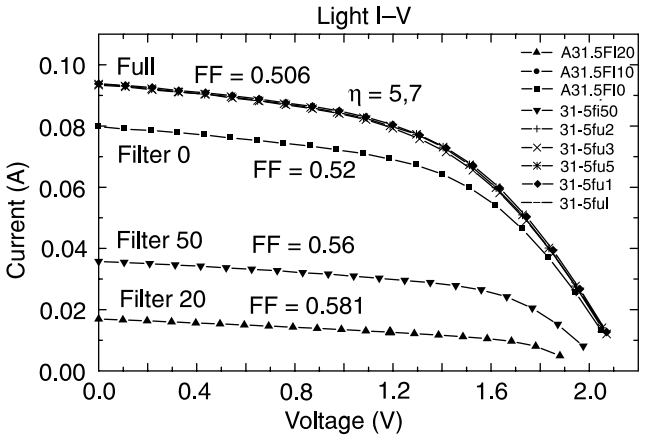

Fig. 18. I–V characteristics of an average triple-junction solar cell on stainless steel, illuminated through filters controlling intensity of light. It is seen the change of FF from 0.506 to 0.581, what indicates the substantial role of serial inner resistance after aging with light of 10 sun for 48 hours.

The resulting comparison of these simulations helps in explanation of an increase in the *FF* value at the decreasing luminance intensity of the incident light. This can be seen in Fig. 18. It is correlated with an existence of a large serial inner resistance of the cell. These are the only qualitative indications, since the single-junction cell model was used to the analysis of the multi-junction structure.

Nevertheless, we expect that the reason of the small *FF* is the oxide inter-layer which was created itself among subsequent cells during displacement of a sample to many vacuum chambers. It shows up that the applied hydrogen-ion cleaning was not sufficient. It is even more evident (the total *FF* degradation) in the case of a tandem cell where the hydrogen-ion cleaning was not applied at all (Fig. 10).

7. Conclusions

In this paper, it was shown that an optimal H dilution, microcrystallization, lower thickness and other operations reduce the SWE effect and increase solar cell stability.

After the analysis of the tandem structures on glass, as well as the structures made on a stainless steel, the target decision was undertaken to manufacture the series of samples in the triple-junction technology on stainless steel.

These cells were manufactured on the 5×5 cm^2 area and consisted of three sandwich-layers as follows: from the back – Al/ZnO mirror, then polycrystalline p-i-n Si structure – made in the higher temperature of about 450°C, then the amorphous p-i-n Si(0.5–1.0%)Ge:H structure, as well as the amorphous p-i-n a-Si:H structure with an ZnO electrode and polysilicone protection.

For the 5×5 cm^2 structures, the following parameters were obtained: FF = ~0.58, V_{oc} = ~2.19 V, I_{sc} = ~6 mA/cm^2, η = ~7.7% at the luminance of 1 sun. At the other hand, for the 25 cm^2 samples it was possible to obtain a 10.5% increase in efficiency.

The measurements of the characteristics I–V from the intensity of luminance showed that the very important role plays the serial resistance, and therefore a modification of the electrode system and an avoidance of the oxide inter-layer can lead to increase in *FF* up to the level of 0.67–0.68.

The irradiation for many hours with intensity of 2 sun caused only about 10% degradations of the properties what is a very good result.

Acknowledgments

The authors would like to thank Prof. C.R. Wronski and the colleagues from Penn State University for preparation of the PECVD samples and measurements used for comparison. The work was done on the basis of the contract PBZ KBN No. 05/T11/98.

References

1. K. Yamamoto, M. Yoshimi, Y. Tawada, Y. Okamoto, A. Nakajima, and S. Igari, "Thin-film poly-Si solar cells on glass substrate fabricated at low temperature", *Appl. Phys.* **A69**, 179 (1999).
2. J. Meier, R. Flückiger, H. Keppner, and A. Shah, "Complete microcrystalline p-i-n solar cell – crystalline or amorphous cell behaviour?", *Appl. Phys. Lett.* **65**, 860 (1994).
3. J. Meier, P. Torres, R. Platz, S. Dubail, U. Kroll, J.A. Selvan, N. Pellaton Vaucher, C. Hof, D. Fischer, H. Keppner, A. Shah, K.D. Ufert, P. Giannoulès, and J. Koehler, "On the way towards high efficiency thin film silicon solar cells by the 'micromorph' concept", *Mat. Res. Symp. Proc.* **420**, 3 (1996).
4. K. Ogawa, K. Saito, M. Sano, A. Sakai, and K. Matsuda, "Microcrystalline silicon thin-film solar cells by very--high-frequency glow discharge", *Technical Digest of the International PVSEC-12*, Jeju, Korea, 343 (2001).
5. A. Kołodziej, P. Krewniak, and R. Tadeusiewicz, "Properties of image sensor structure obtained below 120°C on the foil by reactive magnetron sputtering", *Mat. Res. Soc. Symp. Proc.* **558**, 243–246 (2000).
6. A. Kołodziej, P. Krewniak, and S. Nowak, "Influence of ZnO/p^+a-Si:H microcrystallization and antireflection coatings on pin a-Si:H solar cells performance", *Mat. Res. Soc. Symp. Proc.* **715**, A6.7.1–A6.7.6 (2002).
7. Y. Nasuno, M. Kondo, and A. Matsuda, "Microcrystalline silicon thin-film solar cells prepared at low temperature", *Mat. Res. Symp. Proc.* **664**, A15.5 (2001).
8. U.K. Das, S. Morrison, and A. Madan, "Amorphous and microcrystalline silicon solar cells grown by pulsed PECVD technique", *Mat. Res. Symp. Proc.* **715**, A26.6 (2002).
9. S. Klein, F. Finger, R. Carius, O. Kluth, L.B. Neto, H. Wagner, and M. Stutzmann, "Intrinsic microcrystalline silicon by hot-wire chemical vapour deposition for solar cells applications", *Proc. 17th European Photovoltaic Solar Energy Conference and Exhibition*, Germany, (2001). (in press).
10. S.J. Jones, R. Crucet, X. Deng, D.L. Williamson, and M. Izu, "Preparation of microcrystalline silicon based solar cells at high i-layer deposition rates using a gas jet technique", *Mat. Res. Symp. Proc.* **609**, A4.5 (2000).
11. K. Yamamoto, M. Yoshimi, Y. Tawada, S. Fukuda, T. Sawada, T. Meguro, H. Takata, T. Suezaki, Y. Koi, K. Hayashi, T. Suzuki, and A. Nakajima, "Amorphous and microcrystalline silicon tandem solar cells", *Technical Digest of the International PVSEC-12*, Jeju, Korea, 547 (2001).
12. Y. Nasuno, M. Kondo, and A. Matsuda, "Oxydation effects in microcrystalline silicon", *Mat. Res. Soc. Symp. Proc.* **664**, A15.5 (2001).
13. A. Kołodziej, P. Krewniak, S. Nowak, and E. Leja, "Influence of double-side antireflection coatings and ZnO/ /p^+a-Si:H/ia-Si:H film properties on pin a-Si:H solar cells performance", *Proc. of European Microelectronics Packaging and Interconnection Symposium*, Cracow, Poland, 16–18.06.2002, 358–361 (2002).
14. A. Kołodziej, P. Krewniak, and S. Nowak, "Consideration on wide bandgap amorphous and microcrystalline silicon for solar multijunction cell and x-ray sensor", *Proc. 24th Int. Conf. IMAPS – Poland 2000*, Rytro 25–29.09.2000, Kraków, 335–342 (2000).
15. A. Kołodziej, P. Krewniak, and S. Nowak, "Effectiveness of the n^+/i and p^+/i a-Si:H junctions applied in photovoltaic structures", *Proc. 25th Int. Conf. and Exhibition IMAPS – Poland*, Polańczyk 26–29.09.2001, Rzeszów, 115–118 (2001).
16. A. Kołodziej, P. Krewniak, and S. Nowak, "Efficiency optimization of microcrystalline and amorphous silicon solar cells", *Proc. 26th Int. Conf. of International Microelectronics and Packaging Society*, Warsaw, Poland, 25–27.09.2002, 75–78 (2002).
17. Report for The State Committee for Scientific Research Project No. PBZ KBN 05/T11/98, Kraków, AGH (2003).
18. A. Kołodziej, C.R. Wroński, P. Krewniak, and S. Nowak, "Silicon thin film multijunction solar cells", *Opto-Electron. Rev.* **8**, 71–77 (2000).
19. A. Kołodziej and P. Krewniak, "Improvements of silicon thin film solar cells", *Proc. 6th Framework Programme Workshop*, Ispra, 156–162 (2002).
20. A.S. Ferlauto, G.M. Ferreira, R.J. Koval, J.M. Pearce, C.R. Wronski, and R.W. Collins, "Application of deposition phase diagrams for the optimization of a-Si:H-based materials and solar cells", *Mat. Res. Soc. Symp. Proc.* **762**, A10.1.1–A10.1.12 (2003).
21. S. Guha, "Multijunction solar cells and modules", in *Technology and Applications of Amorphous Silicon*, pp. 252–305, edited by R.A. Street, Berlin, Springer, 2000.
22. S.R. Ovshinsky, "The material basis of efficiency and stability in amorphous photovoltaics", *Solar Energy Materials and Solar Cells* **32**, 443–449 (1994).
23. D.V. Tsu, B.S. Chao, S.R. Ovshinsky, S. Guha, and J. Yang, "Effect of hydrogen dilution on the structure of amorphous silicon alloys", *Appl. Phys. Lett.* **71**, 1317–1319 (1997).
24. A.H. Mahan, J. Yang, S. Guha, and D.L. Williamson, "Structural changes in a-Si:H film crystallinity with high H dilution", *Phys. Rev.* **B61**, 1677–1680 (2000).
25. J. Yang and S. Guha, "Amorphous silicon alloy materials and solar cells near the threshold of microcrystallinity", *Mat. Res. Soc. Symp. Proc.* **557**, 239–250 (1999).
26. J. Koh, A.S. Ferulato, P.I. Rovira, C.R. Wronski, and R.W. Collins, "Evolutionary phase diagrams for plasma-enhanced chemical vapour deposition of silicon thin films from hydrogen-diluted silane", *Appl. Phys. Lett.* **75**, 2286–2288 (1999).
27. J. Yang, K. Lord, S. Guha, and S.R. Ovshinsky, "Amorphous silicon alloy solar cells near the threshold of amorphous to microcrytalline transition", *Mat. Res. Soc. Symp. Proc.* **609**, 2000.
28. S. Guha, J. Yang, D.L. Williamson, Y. Lubianiker, J.D. Cohen, and A.H. Mahan, "Structural, defect, and device behaviour of hydrogenated amorphous Si near and above the onset of microcrystallinity", *Appl. Phys. Lett.* **74**,1860–1862 (1999).

ANNOUNCEMENT and CALL FOR PAPERS

Submit your abstract to this new European meeting

26–30 April 2004
Strasbourg, France

Science • Research • Engineering
Technology • Applications • Commercialization

Present your research and be a part of this unique European event. Photonics Europe will bring together global leaders from all areas of optics/photonics research, development, and commercialization.

Photonics Europe will address the toughest issues facing optical and photonics technology developers today.

Present your research paper in these topical areas:

- Lasers
- Biophotonics
- Optoelectronics
- Nano-Photonics
- Materials
- Metrology
- Sensing
- Micro-Optics
- Packaging
- Micromachining

Plus:

- Special Hot Topics Session

Come to Strasbourg for science and engineering, but stay the week and enjoy the Photonics Hot Topics, 15 cross-disciplinary conferences, an extensive business program, a new European exhibition, and of course the superb Alsatian dining, where new friends and new ideas are just a part of the menu.

Plan now to participate and present your research.

Conferences | spie@spie.org | Tel: +1 360 676 3290

